

# Modeling of Adsorption Properties of Zeolites: Correlation with the Structure

A. Goursot,\* V. Vasilyev, and A. Arbuznikov†

Laboratoire de Matériaux Catalytiques et Catalyse en Chimie Organique, UMR 5618 CNRS, Ecole Nationale Supérieure de Chimie de Montpellier, 8 Rue de l'École Normale, 34053 Montpellier Cédex 1, France

Received: April 9, 1997<sup>⊗</sup>

The adsorption of N<sub>2</sub> and CO in Na X-zeolites has been studied for different framework structures and extraframework cation distributions. To this aim, the cation–molecule system modeling one site has been embedded in a set of external point charges which simulate the zeolite environment of the site and has been treated quantum chemically, using a method based on density functional theory. This procedure has been applied to the 64 cationic sites accessible for adsorption in a crystal unit cell of an ideal X-zeolite with a Si/Al ratio equal to 1. These calculations have shown that only a few cations are favorable for initial adsorption and that those cations are always of type III(III'). Their efficiency depends both on the framework geometry and on their location in the supercages. The analysis of the quantum chemical results in terms of a classical description involving electrostatic and induction interaction energies with the framework has led to the conclusion that the direction of the electric field vector created by the zeolite in the supercages is an important factor determining the zeolite adsorption properties.

## 1. Introduction

Zeolites are aluminosilicate materials that are widely used for size and shape catalysis, hydrocarbon conversion, and sorbing processes. Their physicochemical properties are based on the ability of these open crystalline structures to enclose charged and neutral species within cavities. Their properties are thus strongly related to the structure of the framework and also to the distribution among cages and channels of the cations that are associated with the Al centers. Indeed, those extraframework cations are the active sites for adsorption processes, whereas their neighboring oxygens are involved in base catalysis. Adsorption and desorption studies of small probe molecules like N<sub>2</sub> and CO are used to provide information about cations and basic sites. Those experiments show that the adsorption of molecules within the cages varies with the number and nature of occupied cationic sites.<sup>1–3</sup>

However, there is presently no real understanding of how adsorption properties of zeolites depend on the cation distribution. The major difficulty encountered in the study of such a correlation arises from the incomplete information provided by experimental structure determinations about cationic sites. First, very few structures are known for low-silica zeolites, i.e. for those including a large number of cations.<sup>4</sup> Moreover, the studies concerned with zeolites containing a single type of cations are even more scarce, due to the difficulty of full cationic exchange. Crystal and powder structure determinations provide positions for the cations associated with the probabilities of occupying the various sites, which, very often, do not sum up to the total number of cations. Cation positions vary also with their chemical nature and with the extent of dehydration. Lithium cations are hardly detectable by X-ray diffraction, and sodium cations may not be well differentiated from water molecules. Finally, experimental conditions of preparation and dehydration may induce differences in the solids, leading to different structures and thus different adsorption properties.

For all these reasons, we think that modeling may be an appropriate tool to analyze the relations between adsorption

properties and zeolite structures. Although a large variety of modeling techniques have already been used for the prediction and analysis of zeolite structures and properties, only a very few studies have been devoted to systems including cations other than protons. During the last decade, the main effort has been devoted to H-zeolites, mainly due to their widespread applications in acid catalysis.<sup>5–7</sup> Only recently have some dynamical studies of Na and Ca A-zeolite,<sup>8–10</sup> Na Y-zeolite,<sup>11</sup> and Na and K offretite<sup>12</sup> proposed detailed structures including cation positions. In recent papers, we have shown that the nature of the cation and its location in the framework are essential factors for N<sub>2</sub> and O<sub>2</sub> adsorption.<sup>13,14</sup> In these studies, it was shown that short-range interactions between incoming molecules and framework cations have to be described quantum chemically, whereas long-range interactions are very well approximated as a sum of electrostatic and induction terms. In the latter case, external point charges, representing the zeolite atoms, create a potential and an electric field which interact with the electron density of the incoming gaseous molecule (as a function of its multipole moments and polarizabilities). Hence, this model allows one to approximate the interaction of a molecule with a cationic site within a zeolite using a complete quantum mechanical (QM) treatment of the local adsorption (cation–molecule), including the external perturbation of the set of point charges in the self-consistent solution. Using this embedded cluster model, we study here how N<sub>2</sub> and CO molecules adsorb at all possible cationic sites of a faujasite-type zeolite and to what extent their adsorption properties depend on the zeolite structure, including the cation positions.

For this purpose, three experimental structures of Na X-zeolites of very similar compositions were chosen in order to generate an ideal X-zeolite with a Si/Al ratio of 1, i.e. a composition Na<sub>96</sub>Al<sub>96</sub>Si<sub>96</sub>O<sub>384</sub>. These three structures differ by some geometrical parameters of their framework and also by the positions attributed to the site III cations. The impact of these differences on the adsorption of N<sub>2</sub> and CO will be ascertained by our modeling study.

## 2. Experimental Structures and Models

A detailed analysis of the structures published for Y- and X-zeolites, including various cations,<sup>4,15–21</sup> leads to the conclu-

† Permanent address: Borekov Institute of Catalysis, Siberian Branch of the Russian Academy of Sciences, 630090 Novosibirsk, Russia.

⊗ Abstract published in *Advance ACS Abstracts*, July 1, 1997.

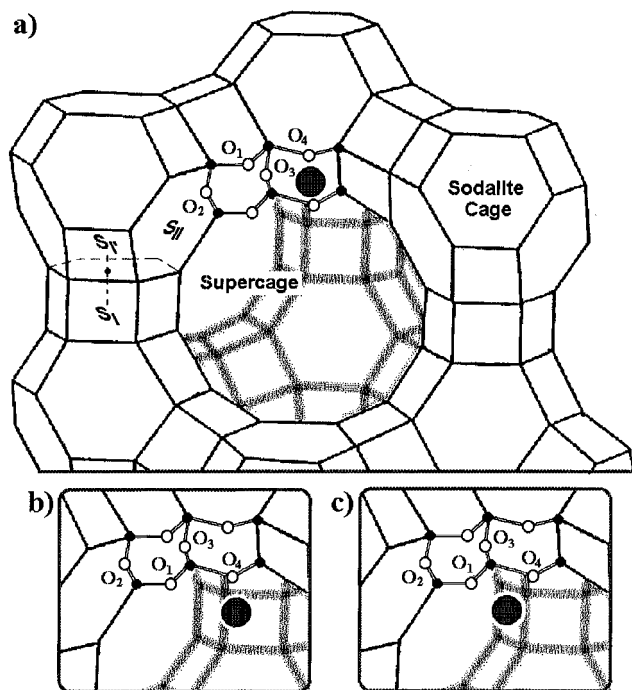


**Figure 1.** Faujasite-type structure with cationic sites: "ideal" site III (a), monocoordinated site III (b), and bicoordinated site III (c).

sion that cations at sites I/I' and II/II' have generally well-defined positions (Figure 1). Cations at sites I(I') are coordinated to three O<sub>3</sub> oxygens in hexagonal prisms (sodalite cages). They are inaccessible to incoming molecules. Site II cations are reachable since they are located in the supercages, coordinated to three O<sub>2</sub> oxygens (6-ring windows of sodalite cages). In contrast, sites II', which are also coordinated to three O<sub>2</sub> oxygens, are not accessible, being located inside sodalite cages.

In dehydrated Y-zeolites (Si/Al > 1.5), the cations are essentially distributed among sites I(I') and II(II'), with a maximum of 32 site II cations available for adsorbing molecules, and very few or no cations at site III(III'), which are also located in the supercages.<sup>4</sup> In contrast, dehydrated X-zeolites (Si/Al < 1.5) are known to contain cations occupying those extra sites in the supercages. There are 48 possible sites III, also called "ideal" sites, coordinated to two O<sub>4</sub> oxygens, whereas 96 additional III' positions are coordinated to O<sub>1</sub> and O<sub>4</sub> oxygens (192 if Al and Si are differentiated) (Figure 1). In fact, there are still other possibilities for such type III cations, for example coordination with three oxygens (O<sub>1</sub>, O<sub>1</sub>, O<sub>4</sub> or O<sub>1</sub>, O<sub>2</sub>, O<sub>4</sub>) or with only one oxygen (O<sub>1</sub> or O<sub>4</sub>). If we assume a full occupancy of 64 cations in sites I(I') and II(II'), then 32 cations have to be accommodated in the type III sites of the supercages for an ideal X-zeolite with a Si/Al ratio equal to 1. This explains the difficulty of the experimental determination of the positions of site III cations, as well as their interest, since X-zeolites are the most efficient systems for adsorption.

For the present study, we have chosen to compare three recent experimental structures referred to as OLS,<sup>21</sup> ALA,<sup>16</sup> and SMO.<sup>15</sup> They contain only sodium cations and correspond to very comparable compositions with 88, 86, and 92 cations for OLS, ALA, and SMO, respectively. Examination of Table 1, which collects the site occupancies for these three X-zeolites, leads to several remarks: (i) there are very few cations in sites I and none in sites II', (ii) the OLS and ALA determinations lead to five extra cations, whereas 21 are missing in the SMO structure, and (iii) the ALA structure contains more cations of type III and less site II cations than the two other structures.

In addition to the above differences between cation distribu-

**TABLE 1: Site Occupancies from X-ray Structures**

structure	composition	site I	site I'	site II	site II'	site III-type	sum
OLS	Na <sub>88</sub>	3	29	32		30	93
ALA	Na <sub>86</sub>	3	21	20		47	91
SMO	Na <sub>92</sub>	3	26	32		10	71

tions, these structures differ also by the location of type III cations in the supercages and by some geometric characteristics of the aluminosilicate framework.

Figure 2 illustrates the different type III sites reported for the OLS (a-c), ALA (e,f), and SMO (d) structures. In the OLS structure, the sodium cations are essentially bicoordinated to O<sub>1</sub>, O<sub>4</sub> oxygens with Al or Si as the T atom and there are also 11 cations coordinated to O<sub>4</sub>. The 10 site III cations reported in the SMO structure are also singly coordinated to O<sub>4</sub>. The ALA structure contains 23 "ideal" bicoordinated cations (on the corresponding four-membered rings) and 24 cations coordinated to only O<sub>4</sub>.

In parallel with these different site III locations, the framework bond lengths and angles show some differences that are more pronounced for the ALA structure with respect to the others. In particular, the O<sub>4</sub>-O<sub>4</sub> distance is much larger, whereas the O<sub>1</sub>-O<sub>1</sub> and O<sub>1</sub>-O<sub>4</sub> distances are smaller, in this structure (Table 2).

In order to compare the adsorption energies of N<sub>2</sub> and CO in these three structures, we have chosen to model them as idealized Na<sub>96</sub>(AlO<sub>2</sub>)<sub>96</sub>(SiO<sub>2</sub>)<sub>96</sub> structures with 32 cations in sites I', II, and III, all framework characteristics being reproduced from the corresponding X-ray data. The 32 type III cations in the OLS structure were distributed as described above, i.e. 11 monocoordinated and 21 bicoordinated. Examination of the geometry around the singly coordinated type III site of the ALA structure has revealed some unrealistic features: (i) a symmetrical arrangement around O<sub>4</sub>, whereas it should be nonsymmetrical; (ii) a quite long O<sub>4</sub>-Na bond length, which also corresponds to a hydrogen bond length, as O<sub>4</sub>-(HOH); (iii) the large number (47) of type III cations, which does not look reasonable, since this large concentration of cations in the supercages leads to a repulsion energy between cations that is twice as large as the repulsion energy when all sites II are populated and only 32 cations are distributed in sites III.

We have thus chosen to model 32 "ideal" type III cations in this ALA structure, instead of the 23 ones in the published structure, and to occupy the 32 available sites II.

In the same spirit, 32 type III cations were distributed among the monocoordinated sites proposed for the SMO structure.

In the three cases, the 32 type III cations were distributed among the corresponding possible locations through the minimization of their mutual Coulomb repulsion, all other cations in sites I' and II being kept fixed. It is worth noting that this minimization can lead to several distributions of type III cations that have comparable stabilities. In the case of the OLS structure, which has the largest number of possible type III sites (240), we have compared the N<sub>2</sub> adsorption energies calculated for three distributions of type III cations that were energetically comparable. The largest difference between the calculated adsorption energies obtained with these three distributions was about 1 kcal/mol, which indicates the largest error related to this procedure. For the ALA and SMO structures, this error is much smaller, due to the much smaller number of possible sites III (48 and 96, respectively).

### 3. Theoretical Method and Calculations

The strategy adopted for these calculations is to model the adsorption of one nitrogen or carbon monoxide molecule in turn

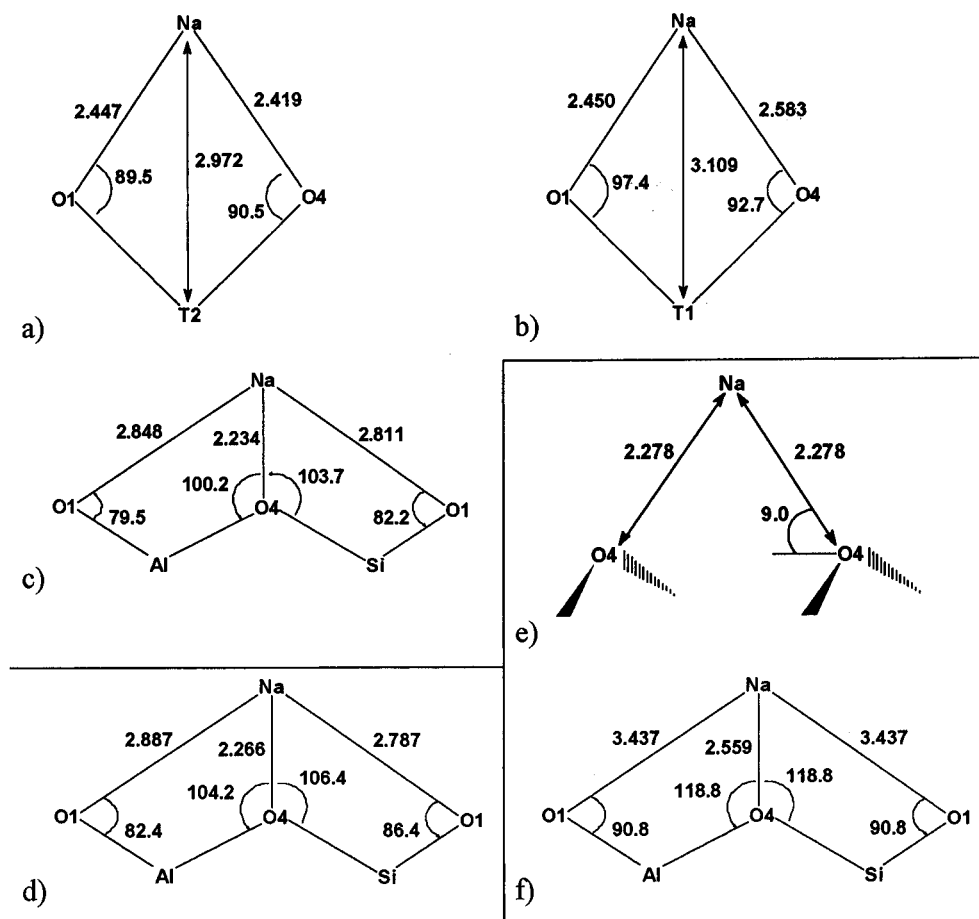


**Figure 2.** Experimental site III positions: OLS structure (a, b, and c), ALA structure (e and f), and SMO structure (d).

**TABLE 2: Some Geometrical Parameters of Na X-Zeolites**

structure	$R(\text{O}_4-\text{O}_4)^a$		$R(\text{O}_1-\text{O}_4)^a$		$R(\text{O}_1-\text{O}_4)^a$ near Si
	$R(\text{O}_4-\text{O}_4)^a$	$R(\text{O}_1-\text{O}_1)^a$	near Al	$\langle \text{O}_1\text{AlO}_4 \rangle^a$	
OLS	3.813	3.827	2.796	109.9	2.610
ALA	4.501	3.655	2.682	99.4	2.682
SMO	3.846	3.846	2.783	109.0	2.581

<sup>a</sup> Distances are in angstroms, and angles are in degrees.

at each cationic site available in the eight supercells of one crystal unit cell, i.e. at all 32 sites II and 32 sites III, for the three structures defined above. In each case, the  $\text{Na}^+-\text{N}_2$  and  $\text{Na}^+-\text{CO}$  systems are treated quantum chemically, including their interaction with 18 143 external point charges, which represent all the atoms of a central unit cell where the adsorption occurs (except the concerned  $\text{Na}^+$  cation) and, in addition, all the atoms of 26 surrounding neutral unit cells. We have verified that this network of charges is sufficient by calculating more extended networks. The error of convergence on the electrostatic potential in the central unit cell is 0.5 kcal/mol only (0.4%), whereas the error on the electric field is 0.0002 au (0.4%).

The interaction of  $\text{Na}^+-\text{N}_2$  ( $\text{Na}^+-\text{CO}$ ) with the zeolite ionic environment includes the Coulomb terms as well as the modifications of the electron density induced by the nonuniform electric field generated by the zeolite (induction terms). Dispersive interactions between the adsorbed molecule and the framework ions are negligible in this case, since their distance is always larger than 9 bohrs. The sodium cations have been fixed at their experimental positions in dehydrated zeolites, which implies that the cation-framework distance is unchanged upon  $\text{N}_2$  ( $\text{CO}$ ) adsorption. There is no experimental evidence for any displacement of cations during adsorption of these

molecules at room temperature, in contrast with their observed mobility when solvated with water molecules. As shown in previous calculations<sup>12,13</sup> and through the electrostatic potential values reported below, the binding energy of the cation with the framework is more than an order of magnitude larger than its binding energy to  $\text{CO}$  and  $\text{N}_2$ . Moreover, this assumption allows an easier comparison of the effect of the structure on the relative adsorption strengths at different sites and in different frameworks.

As in our previous study of adsorption modeling,<sup>13,14</sup> the calculations have been carried out in the framework of density functional theory, using the deMon-KS program.<sup>22-24</sup> All calculations were performed using the gradient-corrected functionals of Perdew and Wang for exchange<sup>25</sup> and Perdew for correlation.<sup>26</sup> Correlation-consistent basis sets of quadruple- $\zeta$  quality have been adopted for N, C, and O,<sup>27,28</sup> in order to avoid BSSE corrections, which are then reduced to less than 0.2 kcal/mol for gaseous  $\text{Na}^+-\text{N}_2$  and  $\text{Na}^+-\text{CO}$  systems, whereas the corresponding auxiliary bases had the pattern (4,4;4,4).<sup>29</sup> For the sodium cation, we have verified that, due to its rare gas electronic configuration, a larger basis set extension, as (6,3,1,1,1,1/4,2,1,1,1/1), has no effect on the calculated adsorption energies. The orbital (6321/521/1) and auxiliary (5,4;5,4) bases were thus employed.<sup>29</sup> The numerical integrations were performed according to the Lebedev scheme, with 64 radial points and a fine angular grid.

Since a linear  $\text{Na}^+$ -molecule geometry is the most favorable in the gaseous state,<sup>13</sup> the incoming molecules were approached to site II cations along the pseudo  $C_3$  axis of the six-membered ring, yielding the optimum distances to  $\text{Na}^+$ , the N-N and C-O bond lengths being kept fixed at their equilibrium values

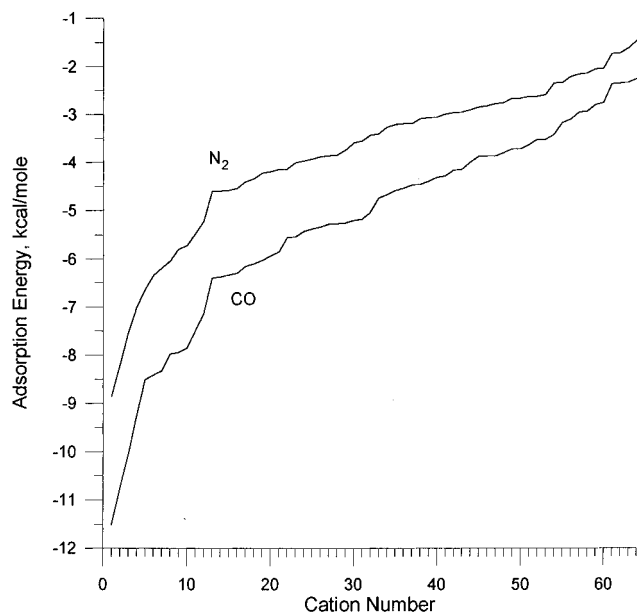


**Figure 3.** Calculated adsorption energies for N<sub>2</sub> and CO in the OLS structure.

optimized for isolated Na<sup>+</sup>-N<sub>2</sub> and Na<sup>+</sup>-CO (1.095 and 1.127 Å, respectively).

For the bicoordinated sites III, the molecules approached along the bisector of the ONaO angle, whereas they were collinear with the O-Na direction for the monocoordinated site III cations.

In the case of nonideal sites III (OLS and SMO structures), other type III cations may prevent a linear approach. The orientation of the incoming molecule has thus been adjusted, minimizing the van der Waals repulsion with the neighboring atoms. In a simplified treatment, N<sub>2</sub> or CO was assumed to be a sphere centered at the middle of the bond, and its repulsion energy with all nonbonded atoms has been evaluated as  $\sum(A_j/R_j^{12})$ , where  $R_j$  is its distance to atom  $j$  and  $A_j$  is the van der Waals parameter, calculated as  $A_j = (a_s a_j)^{1/2}$ . The parameters  $a$  ( $a_s$ ,  $a_j$ ) are defined classically by  $a = 4\epsilon\sigma^{12}$ . The values 0.02957 ( $\epsilon$ ) and 7.5133 kcal mol<sup>-1</sup> ( $\sigma$ ) for this sphere were found to be sufficient to keep the adsorbate from interacting strongly with the other cations (represented by point charges). The corresponding parameters for the other atoms were taken from ref 30.

The charges used for these calculations were -1.2 for O, 1.4 for Al, 2.4 for Si, and 1.0 for Na.<sup>30</sup> It is worth mentioning that the validity of the conclusions that will be drawn from this study are not dependent on the precise values of these atomic charges. Indeed, test calculations have been performed in order to check the effect of the charge values on the calculated adsorption energies. These calculations have shown that the use of another set of charges (derived from MNDO calculations on zeolite models, i.e. -1.0355 for O, 1.245 for Al, 1.897 for Si, and 1.0 for Na) induce a uniform shift of less than 1 kcal/mol for the calculated adsorption energies, leaving unchanged their differences between sites and structures.

## 4. Results and Discussion

**4.1. Adsorption Energies.** The adsorption energies of N<sub>2</sub> and CO at the 64 accessible sites II and III are presented in Figures 3, 4, and 5, for the OLS, ALA, and SMO structures, respectively. They have been evaluated using the expression

$$E_{\text{ads}} = E(Z^- \text{Na}^+ \text{--molecule}) - E(Z^- \text{Na}^+) - E(\text{molecule})$$

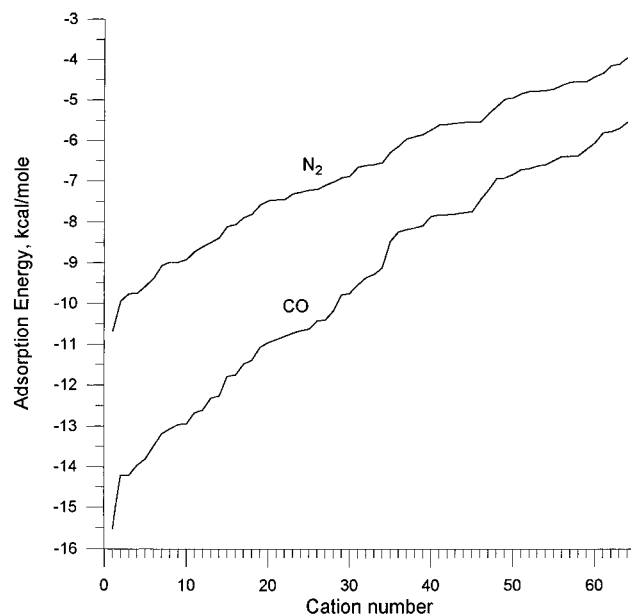


**Figure 4.** Calculated adsorption energies for N<sub>2</sub> and CO in the ALA structure.

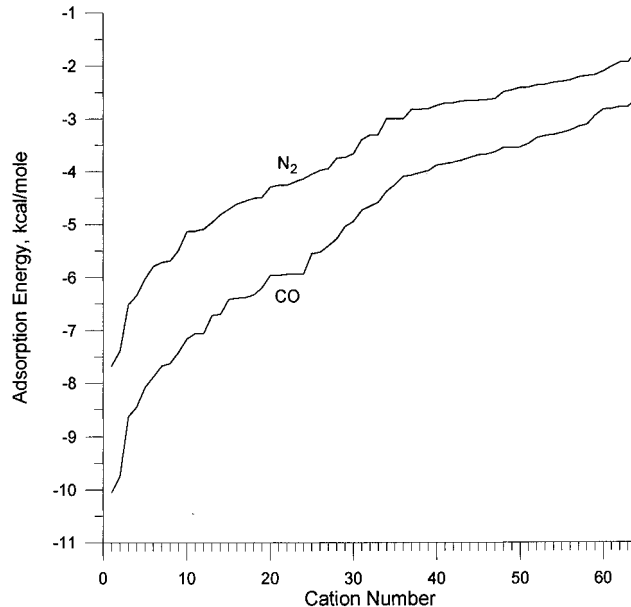


**Figure 5.** Calculated adsorption energies for N<sub>2</sub> and CO in the SMO structure.

where  $E(Z^- \text{Na}^+ \text{--molecule})$  is the total energy of the embedded system at one specific site,  $E(Z^- \text{Na}^+)$  is the total energy of the embedded cation at this site, and  $E(\text{molecule})$  is the total energy for a gaseous N<sub>2</sub> or CO molecule.

Examination of these curves leads to two remarks. First, the most striking result is the very large dispersion of  $E_{\text{ads}}$  values. Indeed, the calculated values spread over 6 (SMO) or 7 (OLS, ALA) kcal mol<sup>-1</sup> for N<sub>2</sub> and 7 (SMO) or 10 (OLS, ALA) kcal mol<sup>-1</sup> for CO. This large range of energies reveals that the local adsorption on a sodium cation, which amounts to -8.15 and -11.4 kcal mol<sup>-1</sup> for N<sub>2</sub> and CO, respectively, without embedding (gaseous state), is strongly perturbed by the environment of the site and that, also, this perturbation is very asymmetric. It is worth noting that the N<sub>2</sub> or CO adsorption energies without embedding are included within the  $E_{\text{ads}}$  values for OLS and ALA structures but remain more stable than the values obtained for the SMO structure. This indicates that, for the former structures, the zeolite environment can weaken or

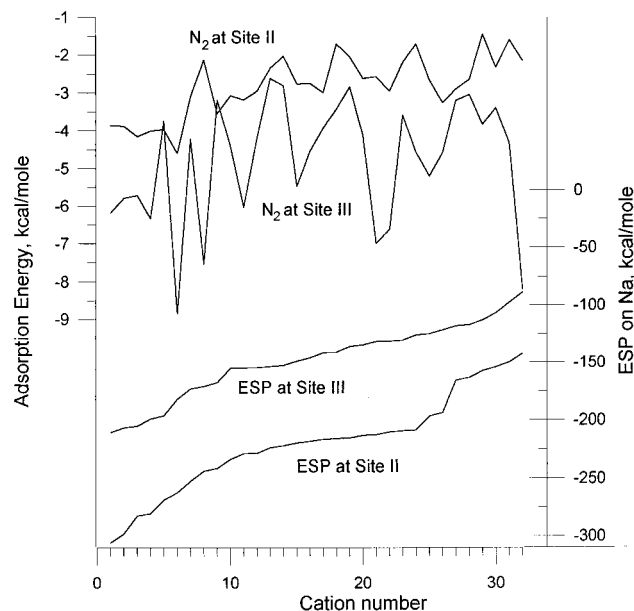


**Figure 6.**  $N_2$  adsorption energies and ESP values at the cation position for sites II and sites III in the OLS structure.

enhance the binding energies of isolated cation–molecule systems, whereas, for the latter structure, there is a weakening effect only.

The second remark concerns the relative adsorption energies for  $N_2$  and CO in the three structures: CO adsorbs more strongly than  $N_2$  on the  $Na^+$  cations and the difference between their adsorption energies increases with the strength of the binding. The fact that CO binds more strongly to  $Na^+$  is due to the additional dipole–cation interaction and is indeed obtained in the gaseous state, where their binding energy difference amounts to  $3.25 \text{ kcal mol}^{-1}$ . For the OLS and ALA structures, this difference is decreased at sites with low adsorption energies and increased at sites with large ones. For the SMO structure, the same trend is followed, but the differences between CO and  $N_2$  binding energies always remain smaller than without embedding.

As a first conclusion, we can say that the embedding generates a large diversity among the accessible sites and may weaken or enhance adsorption properties.

Let us now turn to a more comparative analysis of the adsorption energies on sites II and sites III, which are presented for  $N_2$  in Figures 6, 7, and 8, for OLS, ALA, and SMO structures, respectively. CO adsorption curves are not presented here because they reproduce all the detailed features of Figures 6–8, but with more stable  $E_{\text{ads}}$  values. The ordering of the cationic sites, adopted in these figures, corresponds to that of increasing values for the electrostatic potential (ESP) created by the framework at the cationic sites. The ESP values will be discussed in the next paragraph.

As visible from these figures, the dispersion of  $E_{\text{ads}}$  values for sites II is roughly half this dispersion for sites III, and this is true for all three structures. Moreover, for sites III, the ALA structure shows a significantly smaller dispersion than the two other structures. Those facts correlate with a greater local symmetry around sites II, whichever is the structure, and also for “ideal” sites III (ALA structure).

The second interesting result is that the largest adsorption energies (most stable systems) always correspond to site III cations, for  $N_2$  and CO. Moreover, as shown in the figures, the largest adsorption energies are characteristics of only a few sites of type III. There are also a small number of sites II and sites III which display comparable  $E_{\text{ads}}$  values. However, if

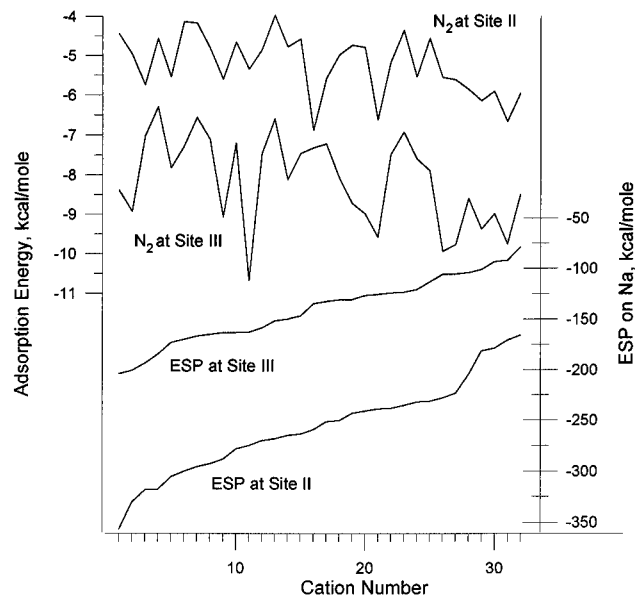


**Figure 7.**  $N_2$  adsorption energies and ESP values at the cation position for sites II and sites III in the ALA structure.

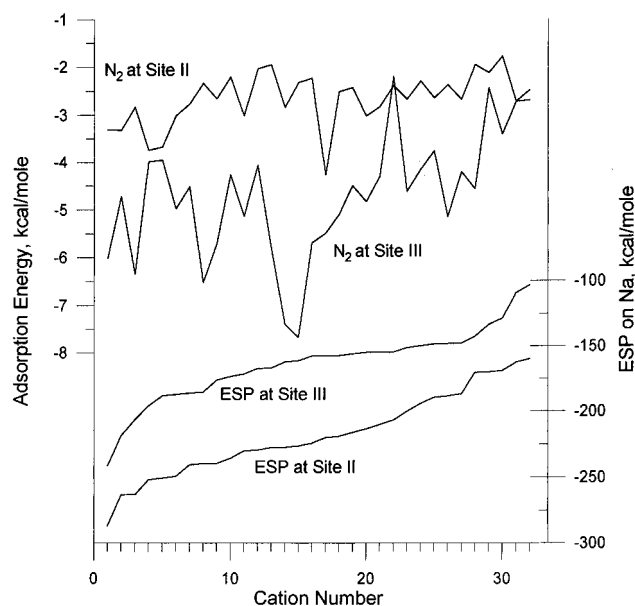


**Figure 8.**  $N_2$  adsorption energies and ESP values at the cation position for sites II and sites III in the SMO structure.

**TABLE 3: Average Adsorption Energies<sup>a</sup> ( $E_{\text{ads,av}}$ ) and Electrostatic Potential Values<sup>a</sup> (ESP<sub>av</sub>) for Sites II and Sites III**

structure	sites II			sites III		
	$(E_{\text{ads}})_{\text{av}N_2}$	$(E_{\text{ads}})_{\text{av}CO}$	ESP <sub>av</sub>	$(E_{\text{ads}})_{\text{av}N_2}$	$(E_{\text{ads}})_{\text{av}CO}$	ESP <sub>av</sub>
OLS	-2.8	-3.9	-219.6	-4.8	-6.6	-147.8
ALA	-5.1	-7.3	-256.0	-8.2	-11.7	-141.0
SMO	-2.7	-3.7	-217.5	-4.7	-6.4	-168.9

<sup>a</sup> Energies in kcal/mol.

the adsorption energies are averaged for sites II and sites III, in order to delineate a trend, the  $(E_{\text{ads}})_{\text{av}}$  values obtained are significantly different for these two types. The average values, presented in Table 3, allow one to delineate several trends: (i)  $N_2$  and CO adsorption are favored at sites III, (ii) the ALA structure is the most efficient for adsorption, whereas the SMO structure is the least efficient, and (iii) the difference between  $N_2$  and CO is larger at sites III than at sites II.

The equilibrium distance between the sodium cations and an incoming molecule does not depend much on the type of site

**TABLE 4: Statistical Adsorption Energies for N<sub>2</sub> and CO at Sites III**

structure	molecule	$\langle E_{\text{ads}} \rangle^a$	number of sites <sup>b</sup>	$p_i$ values
OLS	N <sub>2</sub>	-8.6	3	0.67, 0.23, 0.07
	CO	-11.2	3	0.73, 0.20, 0.06
ALA	N <sub>2</sub>	-9.9	5	0.41, 0.12, 0.09, 0.09, 0.07
	CO	-14.9	4	0.67, 0.08, 0.08, 0.05
SMO	N <sub>2</sub>	-7.4	4	0.55, 0.34, 0.08, 0.06
	CO	-9.8	4	0.55, 0.34, 0.05

<sup>a</sup> Energies in kcal/mol. <sup>b</sup> Only sites with  $p_i > 0.05$  have been taken into account.

nor on the structure, except for site III adsorption in the ALA structure. The average equilibrium distances are calculated at 2.55 Å (Na<sup>+</sup>-N) and 2.63 Å (Na<sup>+</sup>-C), for all sites of the OLS and SMO structures, as well as for sites II of the ALA structure. These distances were reduced to 2.35 and 2.45 Å, respectively, for sites III in the ALA structure. However, it is worthwhile to point out that, in the embedded systems, the binding energy curve is very flat around the equilibrium distance (change of 0.1–0.2 kcal mol<sup>-1</sup> for 0.05 Å). In spite of this imprecision, we can say that, except at sites III in the ALA structure, the zeolite induces some elongation of the Na<sup>+</sup>-N and Na<sup>+</sup>-C distances. For all sites and all structures, the molecule–cation charge transfer is very small, since the Mulliken net charge on the sodium cation ranges from 0.958 to 0.973 for Na<sup>+</sup>-N<sub>2</sub> and from 0.930 to 0.990 for Na<sup>+</sup>-CO. These values are very comparable to the gas phase sodium net charge (0.95 and 0.92 for Na<sup>+</sup>-N<sub>2</sub> and Na<sup>+</sup>-CO, respectively).

Optimization of the N–N and C–O distances has been performed at several sites of the ALA and OLS structures. The vibrational frequencies have also been evaluated. The cation–molecule distances were not changed and the optimized N–N and C–O bond distances were 1.100 ± 0.003 and 1.125 ± 0.003 Å, respectively, which shows no important variation with respect to the equivalent isolated systems. The effect of this optimization on the calculated adsorption energies was less than 0.2 kcal/mol. These results show that although the embedding charges have a large effect on the adsorption energies, the extra perturbation on the geometries induced by the zeolite in the adsorbed molecules is very small.

A more realistic description of the adsorption process is given by a statistical evaluation of the site occupancies at 298 K, which are calculated as

$$p_i = P_i / P_{\text{tot}}$$

where  $P_i$  is the Boltzmann factor ( $P_i = \exp(-E_{\text{ads}}(i)/kT)$ , which represents the relative weight of site  $i$  in the statistical adsorption energy  $\langle E_{\text{ads}} \rangle$ ,  $P_{\text{tot}}$  is the sum of the 64  $P_i$  values, and  $E_{\text{ads}}(i)$  is the adsorption energy at site  $i$ . The statistical adsorption energy  $\langle E_{\text{ads}} \rangle$  is then evaluated as  $\sum(p_i E_{\text{ads}}(i))$ .

The results (Table 4) show that, indeed, few sites contribute with substantial efficiencies, and, as expected from the above, these sites are all of type III. There are only three to five sites, according to the structure, which contribute with a probability larger than 5%. The trends deduced from the analysis of the average  $E_{\text{ads}}$  values for sites III (Table 3) are still valid when the  $\langle E_{\text{ads}} \rangle$  energies are considered.

From these results, we can already conclude that, whichever is the type of position for site III cations, i.e. “ideal” (ALA), mainly bicoordinated (OLS), or monocoordinated (SMO), they are the most probable sites for initial adsorption. We can thus propose that this is the reason why X-zeolites are more efficient for N<sub>2</sub> and CO adsorption than Y-zeolites, where essentially

sites II are populated. This conclusion is in agreement with several experimental results that compare adsorption properties of X- and Y-zeolites.<sup>1,2,31</sup>

As already precised, the purpose of this work is to analyze the incidence of the framework geometry and cation distribution on the adsorption properties of Na X-zeolites, without predicting accurate adsorption energies. We are indeed aware that the choice of external charge values and the necessary distribution of cations among all possible sites III are two sources of errors of the absolute values of adsorption energies. Moreover, different structures produce different calculated adsorption energies. However, keeping these restrictions in mind, we find it interesting to check if the values calculated with the embedded cluster model are in a reasonable range with respect to experimental values.

The  $\langle E_{\text{ads}} \rangle$  values are obtained directly from differences of electronic total energies for the isolated compounds and the complex. In order to compare with experimental enthalpies of adsorption, we have assumed that ideal gas conditions apply. The change in internal energy due to adsorption has been determined by subtracting the sum of the internal energies of the isolated species (Z<sup>-</sup>Na<sup>+</sup>, molecule) from the internal energy of the adsorbed model. For the latter, there are no rotational and translational degrees of freedom, whereas their contribution is  $(5/2)RT$  for the gaseous molecules. The zero point energy contributions have been evaluated using the vibrational frequencies calculated in each structure for the site with the largest adsorption energy. The corrections were 1.05, 0.77, 0.75 kcal/mol for N<sub>2</sub> and 1.19, 0.76, 0.74 kcal/mol for CO, in the ALA, OLS, and SMO structures, respectively. The contributions due to the effect of temperature on vibrational populations were 0.92, 1.09, 1.00 kcal/mol for N<sub>2</sub> and 0.87, 1.16, 0.97 kcal/mol for CO, respectively. The energy changes were converted to enthalpy by adding  $RT$ . For a temperature of 298 K, the evaluated adsorption enthalpies are thus within -6.5 to -8.7 kcal/mol for N<sub>2</sub> and -9.0 to -13.7 kcal/mol for CO. These values should represent the upper limit for adsorption energies since our models correspond to the largest Al (and thus cationic) content. The agreement with experimental isosteric heats of adsorption is very reasonable. Indeed, values of 6.3 for N<sub>2</sub><sup>32</sup> and 7.8 kcal/mole for CO<sup>33</sup> have been proposed for initial heats of adsorption in dehydrated Na X-zeolites.

The adsorption energies obtained with the three structures spread over a range of 3 and 5 kcal/mol for N<sub>2</sub> and CO, respectively. In spite of the errors related to our calculations (see sections 2 and 3), we think that these differences are not meaningless. The SMO and ALA structures, which have the lowest and the highest efficiency for adsorption, display significant differences in their framework geometries and in their site III positions. In contrast, the OLS and SMO structures have very similar framework geometries and differ essentially by 22 bicoordinated (OLS) or monocoordinated (SMO) site III cations. Although the error bar on adsorption energies is larger for the OLS structure, because of the large number of possibilities in distributing the 32 cations among sites III, we think that this structure is indeed more efficient than the SMO one, and the reason must be their difference in site III positions. Hence, both the framework geometries and the locations of site III cations play a role in the adsorption capacity of a zeolite, and it is, presently, hardly possible to delineate their relative influence.

**4.2. Electrostatic Potential (ESP).** It is well-known that ESPs give a more realistic description of electron donor properties of a system than atomic net charges. In previous work on zeolites, the electron density of the framework was

described with a QM method and the positions of the ESP wells were used as approximate cation locations, before geometry optimization.<sup>12,34</sup> The ESP minima were shown to be good approximations for the optimized cation positions, whereas their relative depths gave a valuable estimate of their relative binding energies to the framework.

In this paper, the ESP values are calculated from the set of point charges that constitutes the embedding of each cationic site. This is a very crude description of the electron density of the zeolite, but it is worth mentioning that these charge values have themselves been evaluated through a fitting of ESP values obtained from QM calculations. We will thus consider the ESP values calculated at each cationic site (types II and III) as a measure of the local bond strength between the framework and the cation (represented by a +1 charge).

Examination of Figures 6–8 shows that there is a clear trend concerning the electrostatic potential at the cation position and the cation–molecule interaction energy, which distinguishes sites II and sites III. There is no individual correlation between  $E_{\text{ads}}$  and ESP values, in the sense that two cations may have comparable ESP values, whichever is the type of site, but correspond to very different adsorption energies. However, there is a general trend for the three structures concerning the behavior of ESP values: they are smaller for sites III than for sites II (Table 3), leading to the proposal that larger adsorption energies are related with smaller ESPs. In fact, this trend seems very reasonable in the sense that if a cation is more strongly bonded to a more basic framework (large ESP), its electron deficiency is decreased, leading to a smaller interaction energy with  $\text{N}_2$  or  $\text{CO}$ . This decrease of the electrophilic character of the cation is not obtained through a full quantum treatment of the whole zeolite, i.e. involving charge transfer and exchange–correlation effects. It is indeed modeled by the action of an external negative potential in the QM treatment of the cation (alone and in the complex system), which screens its adsorption capacity. This screening changes with the cation location in the framework and also with the framework geometry itself.

This result correlates very well with the existence of an intrinsic framework basicity which has been proposed as being able to enhance basic properties of some zeolites with respect to what would be expected from their Al content.<sup>35</sup> We can say that the framework structure around sites II has, in general, a larger aptitude to attract the cation, screening more than at sites III its electrophilic character.

However, the correlation between the ESP value at a cationic site and the adsorption energy at this site cannot be more than a general trend since the external potential created by the embedding interacts not only with the cation but also with the whole electron density of the complex cation–molecule. The action of the embedding provides then electrostatic energy terms involving all permanent multipole moments of this system.<sup>36</sup> As for the ESP term (related to the monopole), these contributions vary with the cationic site and with the structure.

Besides these electrostatic terms, the embedded model includes also the interaction of the surrounding with the electric dipole moments it has induced in the cation–molecule complex. The induced dipoles result from the distortion of the electronic distributions of  $\text{Na}^+-\text{N}_2$  and  $\text{Na}^+-\text{CO}$  in response to the electric field created by the embedding. It is thus interesting to analyze in some detail the electric field values and directions that are produced in the different structures.

**4.3. Electric Field.** The action of a uniform electric field  $\mathbf{F}$  on a system provides a contribution to its total energy, which, limited to the second order in  $\mathbf{F}$ , is approximated by  $-\boldsymbol{\mu}\mathbf{F} -$

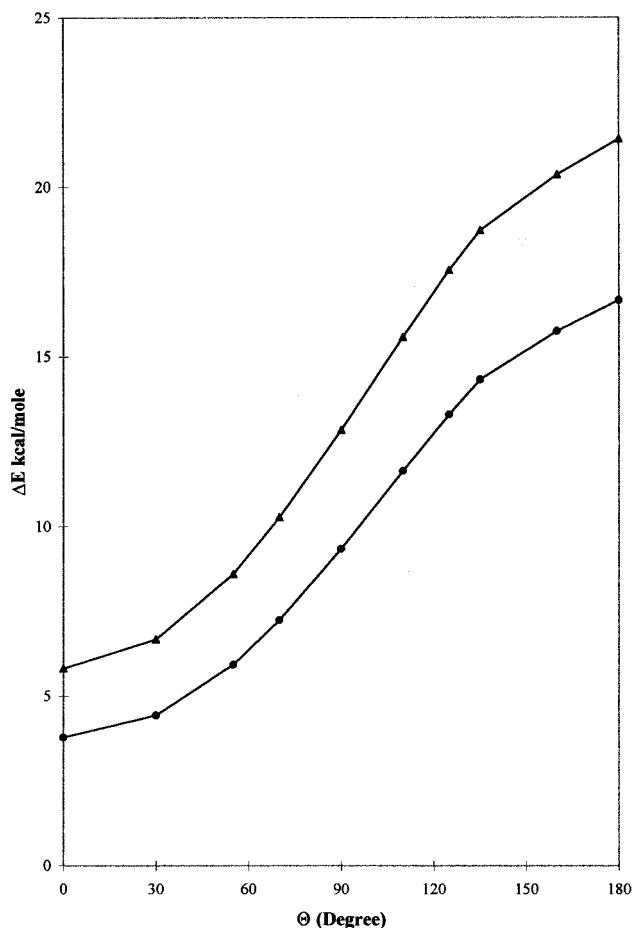


**Figure 9.** Variation of  $\text{Na}^+\text{N}_2$  (circles) and  $\text{Na}^+\text{CO}$  (triangles) adsorption energies with the direction  $\Theta$  of the electric field applied to the system.

$(1/2)\boldsymbol{\alpha}:\mathbf{F}^2$ , where  $\boldsymbol{\mu}$  is the permanent dipole moment of the system and  $\boldsymbol{\alpha}$  its polarizability tensor.

Classically, the first term contributes to the electrostatic energy, whereas the second one is the so-called induction energy. In fact, the electric field in the supercages is nonuniform, varying in modulus and direction, going from the cations to the middle of the supercages and also from one cationic site to another. The nonuniformity of the field involves energy terms proportional to the electric field gradient, the quadrupole moment, and the quadrupole polarizability of the system.

In order to delineate the role of the electric field generated by the zeolite embedding on the  $\text{N}_2$  and  $\text{CO}$  adsorption energies, we have applied a uniform electric field of 0.02 au to  $\text{Na}^+-\text{N}_2$  and  $\text{Na}^+-\text{CO}$ , and the new binding energies of  $\text{N}_2$  and  $\text{CO}$  have been estimated, in a way similar to the above  $E_{\text{ads}}$  values:

$$\Delta E = |E(\text{Na}^+-\text{molecule})^{\text{F}} - E(\text{Na}^+)^{\text{F}} - E(\text{molecule})|$$

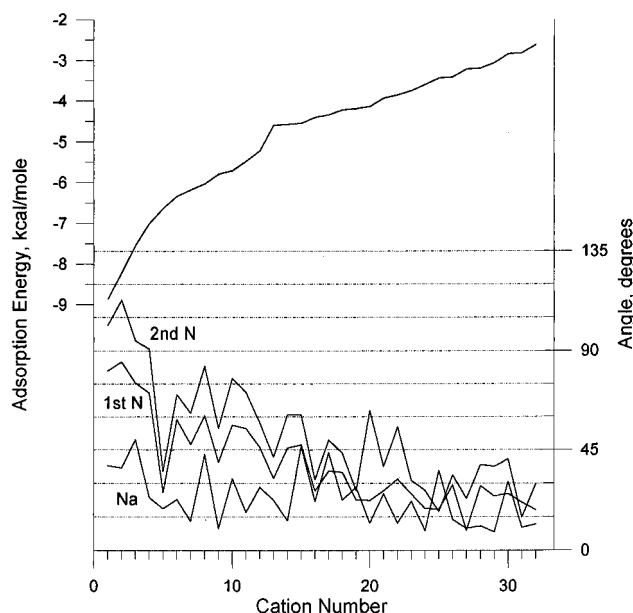
where the superscript F indicates that the energy is calculated in the presence of the electric field.

A value of 0.02 au has been chosen for the absolute value of the electric field because it is included in the range 0.01–0.035 of the field values generated by the surroundings within a distance of 2.6 Å from the cations. The action of the field vector has been studied as a function of its direction, with the angle  $\Theta = 0^\circ$  when the vector is directed from the molecule toward the cation. The results, presented in Figure 9, show that the binding energies of  $\text{N}_2$  and  $\text{CO}$  to  $\text{Na}^+$  are very sensitive to the direction of the field, which is understandable, due to the large polarizability of these systems (Table 5). As could be expected,

**TABLE 5: Effect of an External Uniform Electric Field on  $\text{Na}^+\text{N}_2$  and  $\text{Na}^+\text{CO}$  Properties, as a Function of the Field Direction  $\theta$** 

properties <sup>a</sup>		$ F  = 0$	$ F  = 0.02$ $\theta = 0^\circ$ <sup>b</sup>	$ F  = 0.02$ $\theta = 90^\circ$ <sup>b</sup>	$ F  = 0.02$ $\theta = 180^\circ$ <sup>b</sup>
$\Delta E$	$\text{N}_2$	-8.2	-3.8	-9.3	-16.9
	$\text{CO}$	-11.4	-5.8	-12.8	-21.4
$q_{\text{Na}^+}$	$\text{N}_2$	0.953	0.967	0.951	0.930
	$\text{CO}$	0.924	0.947	0.920	0.885
	$q_{\text{N1}}$	0.013	0.020	0.015	0.000
	$q_c$	0.098	0.150	0.100	0.057
	$q_{\text{N2}}$	0.034	0.013	0.034	0.070
	$q_0$	-0.022	-0.097	-0.020	0.058
$\mu$	$\text{N}_2$	1.32	0.49	1.41	2.19
	$\text{CO}$	1.60	0.74	1.72	2.56
$\alpha_{\parallel}$	$\text{N}_2$	16.5			
	$\text{CO}$	16.8			
$\alpha_{\perp}$	$\text{N}_2$	9.7			
	$\text{CO}$	11.6			

<sup>a</sup>  $\Delta E$  is the adsorption energy in kcal/mol,  $q_{\text{Na}^+}$ ,  $q_{\text{N1}}$ ,  $q_{\text{N2}}$ ,  $q_c$ , and  $q_0$  are the Mulliken atomic net charges in electron;  $\mu$  is the dipole moment in D;  $\alpha_{\parallel}$  and  $\alpha_{\perp}$  are the parallel and perpendicular polarizabilities in au. <sup>b</sup> The electric field  $|F|$  is in au;  $\theta = 0$  corresponds to the electric field vector colinear with  $\text{N}_2\text{-N}_1\text{-Na}^+$  ( $\text{O-C-Na}^+$ ) and pointing toward  $\text{Na}^+$ .

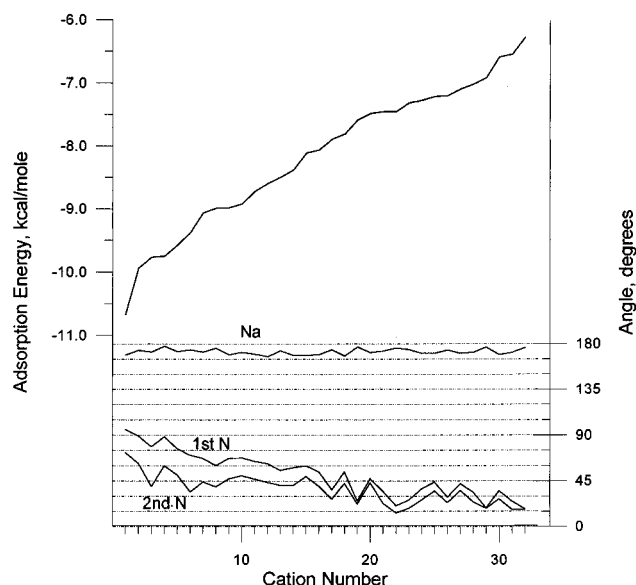
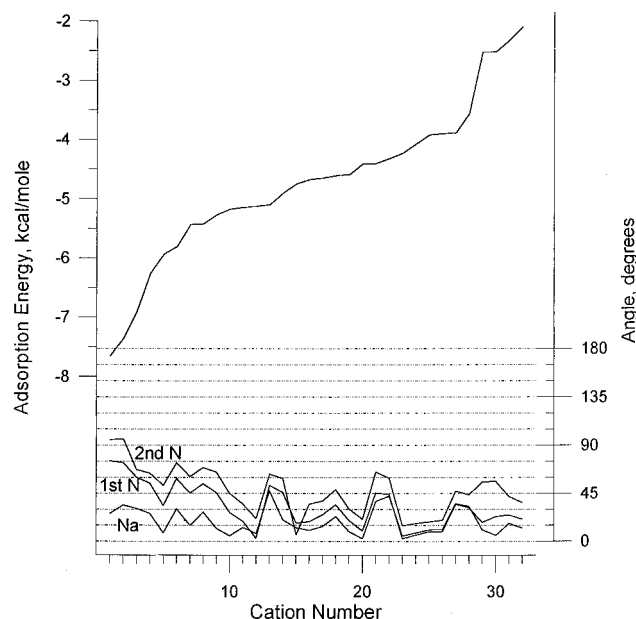
**Figure 10.**  $\text{N}_2$  adsorption energies as a function of the electric field direction at sites III in the OLS structure.

a field directed from the cation to the molecule is very favorable for adsorption, due to the induced electric dipole moment which pulls the electron density in the direction opposite to the field. In that case, both the  $|\mu| \cdot |F| \cos \Theta$  and induction terms contribute to stabilize the  $\text{Na}^+\text{-molecule}$  system.

The curves obtained for  $\text{Na}^+\text{-N}_2$  and  $\text{Na}^+\text{-CO}$  also show that the binding energy difference between the two systems is the smallest for  $\Theta = 0^\circ$  and the largest for  $\Theta = 180^\circ$ , due to the permanent dipole contribution, with the largest  $\mu$  value for  $\text{Na}^+\text{-CO}$ .

Examination of the Mulliken atomic charges (Table 5) confirms that, indeed, the field direction that is the least favorable for adsorption ( $\Theta = 0^\circ$ ) corresponds to the largest positive charge on  $\text{Na}^+$ , i.e. the smallest charge transfer from the molecule to the cation, with the opposite behavior for  $\Theta = 180^\circ$ .

In order to appreciate to what extent the adsorption energies are correlated to the electric field direction in the zeolite, we

**Figure 11.**  $\text{N}_2$  adsorption energies as a function of the electric field direction at sites III in the ALA structure.**Figure 12.**  $\text{N}_2$  adsorption energies as a function of the electric field direction at sites III in the SMO structure.

have reported in Figures 10–12 the variation of  $\text{N}_2$  adsorption energies at sites III for the three structures, together with the field direction (indicated by the  $\Theta$  angle defined above), at the  $\text{Na}^+$ , first and second nitrogen positions.

From these figures, it is clear that the OLS and SMO structures have comparable field directions, although OLS curves for  $\text{N}_1$  and  $\text{N}_2$  are slightly shifted toward larger  $\Theta$  values. The features are different for the ALA structure, with a smoother variation of  $E_{\text{ads}}$  values with the electric field direction at  $\text{N}_1$  and  $\text{N}_2$  and, essentially, a constant  $\Theta$  value of  $180^\circ$  at the sodium positions.

Moreover, for the three structures, there is a clear trend of decreasing adsorption energies with a decreasing  $\Theta$  value from  $90^\circ$  to  $0^\circ$  at the nitrogen positions. The statistical  $\langle E_{\text{ads}} \rangle$  values are all related to  $\Theta$  values very close to  $90^\circ$ . The largest difference between the ALA structure and the two others corresponds to a more favorable field direction at the sodium position ( $\Theta = 180^\circ$ ), which favors its electron acceptor character in the direction of the incoming molecule. This favorable  $\Theta$

value at the cation position for the ALA structure implies also that the electric field gradient is larger than that for the OLS and SMO structures, in this region of space (cation–molecule). Since the quadrupole electrostatic term involves the electric field gradient, this trend also favors the enhancement of the N<sub>2</sub> and CO adsorption energy in the ALA structure.

Finally, if we go back to Figures 3–5 and compare with Figure 9, we can now explain the variation of the energy difference between CO and N<sub>2</sub> curves in the embedded model: the small difference of energy corresponds to sites II, where the adsorption energy is the smallest, whereas the largest difference corresponds to the most efficient sites III, where the adsorption energy is the largest. This variation correlates with the direction of the electric field for the corresponding sites:  $\Theta$  values smaller than 10° for the least efficient sites II and  $\Theta$  values of around 90° for the most efficient sites III. Moreover, the action of a favorable direction of the electric field explains why the ALA structure, which is already the most favorable for N<sub>2</sub> adsorption, still enhances the CO adsorption energy, through the existence of the permanent dipole–field interaction.

The electric field direction is thus indeed one governing factor of the largest efficiency of some site III cations.

## 5. Conclusion

The theoretical model we have used for this study provides a quantum mechanical treatment of the cation–molecule system, perturbed by different external potentials, modeling the different sites. Hence, it allows the accurate evaluation of the effect of these different perturbations on the binding energies with N<sub>2</sub> and CO molecules. Since the embedding charges are at sufficiently large distances, the QM results can be rationalized using the classical decomposition of the long-range interaction energy between two systems, where one system is reduced to a set of point charges. Among the energy terms, only the electrostatic and induction contributions have been considered.

This analysis has allowed one to delineate how the zeolite structure can modulate the adsorption capacity of the cations, as well as the binding ability of the incoming molecules.

Our calculations have shown that the zeolite structure induces a strong dissymmetry among the different available cations. This dissymmetry, as well as the influence of the electric field direction cannot be reproduced using a small cluster modeling the zeolite. Indeed, in contrast with a previous proposal based on a cluster study,<sup>13</sup> the present embedded model shows that the role of the zeolite cannot be reduced to a screening of the cation's electrophilic character. The long-range electrostatic terms can also enhance the Na<sup>+</sup>–N<sub>2</sub> and Na<sup>+</sup>–CO binding energies. This is what happens, at some favored sites, where the adsorption energies are larger than for an isolated cation.

The analysis of the results obtained with the three structures of faujasite-type chosen for this study has demonstrated that favored cationic sites for adsorption are always of type III. This conclusion correlates very well with the upfield displacements of the <sup>129</sup>Xe NMR chemical shifts in X-zeolites with respect to Y-zeolites.<sup>37,38</sup> Moreover, a detailed study of the electric field direction in the space surrounding cations has shown that the most favorable conditions for adsorption are fulfilled only for a few site III cations, which, indeed, correspond to the largest adsorption energies calculated quantum chemically.

The zeolite structure has thus a substantial effect on N<sub>2</sub> and CO adsorption energies since different structures may lead to quite different adsorption energies. From the present results, it is hardly possible to ascertain whether it is the cation distribution or the framework geometry which is the most important factor. Further calculations are in progress in order

to reach a more detailed understanding of the correlation between the zeolite structure and its adsorption properties.

**Acknowledgment.** A.A. and V.V. thank Elf Aquitaine for a post-doctoral fellowship. The authors thank Dr. F. Fajula for very fruitful discussions and the Centre Universitaire Sud de Calcul de Montpellier for the provision of computational resources.

## References and Notes

- (1) Bao Liu Su; Barthomeuf, D. *Appl. Catal. A* **1995**, *124*, 81.
- (2) Seidel, A.; Boddenberg, B. *Z. Naturforsch.* **1995**, *50*, 199.
- (3) Laspéras, M.; Cambon, H.; Brunel, D.; Rodriguez, I.; Geneste, P. *Microporous Mater.* **1996**, *7*, 61.
- (4) Mortier, W. J. *Compilation of Extra Framework Sites in Zeolites*; Butterworth-Heinemann: London, 1982.
- (5) Catlow, C. R. A., Ed. *Modeling of Structure and Reactivity in Zeolites*; Academic Press: London, 1982.
- (6) Catlow, C. R. W.; Bell, R. G.; Gale, J. D.; Lewis, D. W. In *Zeolites: A Refined Tool for Designing Catalytic Sites*; Bonneviot, L., Kaliaguine, S., Eds.; Elsevier: Amsterdam, 1995; p 87.
- (7) Teunissen, E. H.; Jansen, A. P. J.; van Santen, R. A. *J. Phys. Chem.* **1995**, *99*, 1873.
- (8) Moon, G. K.; Choi, S. G.; Kim, H. S.; Lee, S. H. *Bull. Korean Chem. Soc.* **1992**, *13*, 317.
- (9) Moon, G. K.; Choi, S. G.; Kim, H. S.; Lee, S. H. *Bull. Korean Chem. Soc.* **1994**, *14*, 305.
- (10) Lee, S. H.; Moon, G. K.; Choi, S. G.; Kim, H. S. *J. Phys. Chem.* **1994**, *98*, 1561.
- (11) Schrimpf, G.; Schlenkrich, M.; Brickmann, J.; Bopp, P. *J. Phys. Chem.* **1992**, *96*, 7404.
- (12) Campana, L.; Selloni, A.; Weber, J.; Goursot, A. *J. Phys. Chem.* **1995**, *99*, 16351.
- (13) Pápai, I.; Goursot, A.; Fajula, F.; Plee, D.; Weber, J. *J. Phys. Chem.* **1995**, *99*, 12925.
- (14) Goursot, A.; Pápai, I.; Vasilyev, V.; Fajula, F. In *Zeolites: A Refined Tool for Designing Catalytic Sites*; Bonneviot, L., Kaliaguine, S., Eds.; Elsevier: Amsterdam, 1995; p 109.
- (15) Smolin, Yu. I.; Shepelev, Yu. F.; Butikova, I. K.; Petranovskii, I. K. *Kristallografia* **1983**, *28*, 72.
- (16) Al-Ajdah, G. N. D.; Al-Rished, A. A.; Beagley, B.; Dwyer, J.; Fitch, F. R.; Ibrahim, T. K. *J. Inclusion Phenom.* **1985**, *3*, 135.
- (17) Forano, C.; Slade, R. C. T.; Krogh Andersen, E.; Krogh Andersen, G.; Prince, E. *J. Solid State Chem.* **1989**, *82*, 95.
- (18) Shepelev, Yu. F.; Anderson, A. A.; Smolin, Yu. I. *Zeolites* **1990**, *10*, 61.
- (19) Shepelev, Yu. F.; Butikova, I. K.; Smolin, Yu. I. *Zeolites* **1991**, *11*, 287.
- (20) Koller, H.; Burger, B.; Schneider, A. M.; Engelhardt, G.; Weitkamp, J. *Microporous Mater.* **1995**, *5*, 219.
- (21) Olson, D. H. *Zeolites* **1995**, *15*, 439.
- (22) St-Amant, A.; Salahub, D. R. *Chem. Phys. Lett.* **1990**, *169*, 387.
- (23) St-Amant, A. Ph.D. Thesis, Université de Montréal, 1991.
- (24) Daul, C.; Goursot, A.; Salahub, D. R. In *Numerical Grid Methods and Their Application to Schrodinger's Equation*; Cerjan, C., Ed.; NATO ASI Series 412; Kluwer Academic Press: Dordrecht, 1993; p 153.
- (25) Perdew, J. P.; Wang, Y. *Phys. Rev. B* **1986**, *33*, 8800.
- (26) Perdew, J. P. *Phys. Rev. B* **1986**, *33*, 8822; *Phys. Rev. B* **1986**, *B34*, 7406E.
- (27) Dunning, T. H., Jr. *J. Chem. Phys.* **1989**, *90*, 1007.
- (28) Woon, D.; Dunning, T. H., Jr. *J. Chem. Phys.* **1993**, *98*, 1358.
- (29) Godbout, N.; Salahub, D. R.; Andzelm, J.; Wimmer, E. *Can. J. Chem.* **1992**, *70*, 560.
- (30) *Catalysis 4.0 Software User Manual*; Biosym Technologies Inc.: San Diego, 1993.
- (31) Barthomeuf, D. *Stud. Surf. Sci. Catal.* **1991**, *65*, 157.
- (32) Breck, D. W. *Zeolite Mol. Sieves*; John Wiley: New York, 1984.
- (33) Haber, J.; Ptaszynski, J.; Sloczynski, J. *Bull. Acad. Pol. Sci., Ser. Sci. Chim.* **1975**, *30*, 709.
- (34) Pápai, I.; Goursot, A.; Fajula, F.; Weber, J. *J. Phys. Chem.* **1994**, *98*, 4654.
- (35) Barthomeuf, D. *Catal. Rev.* **1996**, *38*, 521.
- (36) Langlet, J.; Claverie, P.; Caron, F.; Boeue, J. C. *Int. J. Quantum Chem.* **1981**, *20*, 299.
- (37) Grosse, R.; Burmeister, R.; Boddenberg, B.; Gedeon, A.; Fraissard, J. *J. Phys. Chem.* **1991**, *95*, 2443.
- (38) Grosse, R.; Gedeon, A.; Watermann, J.; Fraissard, J.; Boddenberg, B. *Zeolites* **1992**, *12*, 909.